Received: 1 January 2022 | Revised: 6 February 2022 | Accepted: 21 February 2022

DOI: 10.1002/idm2.12022

RESEARCH ARTICLE

Interdisciplinary Materials — Open Access WILEY

Nitrogen-doped tin oxide electron transport layer for stable perovskite solar cells with efficiency over 23%

Yanping Mo[1,2] | Chao Wang[1] | Xuntian Zheng[1] | Peng Zhou[1] | Jing Li[1] | Xinxin Yu[1] | Kaizhong Yang[1] | Xinyu Deng[3] | Hyesung Park[4] | Fuzhi Huang[1,2] | Yi-Bing Cheng[1,2]

[1]State Key Laboratory of Advanced Technology for Materials Synthesis and Processing, Wuhan University of Technology, Wuhan, P. R. China

[2]Solar Hydrogen Production Lab, Foshan Xianhu Laboratory of the Advanced Energy Science and Technology Guangdong Laboratory, Foshan, P. R. China

[3]International School of Materials Science and Engineering, Wuhan University of Technology, Wuhan, P. R. China

[4]Department of Materials Science and Engineering, Graduate School of Semiconductor Materials and Devices Engineering, Perovtronics Research Center, Low Dimensional Carbon Materials Center, Ulsan National Institute of Science and Technology, Ulsan, Republic of Korea

Correspondence

Hyesung Park, Department of Materials Science and Engineering, Graduate School of Semiconductor Materials and Devices Engineering, Perovtronics Research Center, Low Dimensional Carbon Materials Center, Ulsan National Institute of Science and Technology, Ulsan 44919, Republic of Korea.
Email: hspark@unist.ac.kr

Fuzhi Huang, State Key Laboratory of Advanced Technology for Materials Synthesis and Processing, Wuhan University of Technology, Wuhan 430070, P. R. China.
Email: fuzhi.huang@whut.edu.cn

Funding information

National Natural Science Foundation of China, Grant/Award Numbers: 21875178, 52172230, 91963209; Foshan Xianhu Laboratory of the Advanced Energy Science and Technology Guangdong Laboratory, Grant/Award Numbers: XDT2020-001, XHT2020-005; Fundamental Research Funds for the Central Universities, Grant/Award Number: WUT: 202443004; Ministry of Science and Technology of the People's Republic of China, Grant/Award Numbers: 2017YFE0131900, 2019YFE0107200

Abstract

Tin oxide has made a major breakthrough in high-efficiency perovskite solar cells (PSCs) as an efficient electron transport layer by the low-temperature chemical bath deposition method. However, tin oxide often contains pernicious defects, resulting in unsatisfactory performance. Herein, we develop high-quality tin oxide films via a nitrogen-doping strategy for high-efficiency and stable planar PSCs. The aligned energy level at the interface of doped SnO_2/perovskite, more excellent charge extraction and reduced nonradiative recombination contribute to the enhanced efficiency and stability. Correspondingly, the power conversion efficiency of the devices based on N-SnO_2 film increases to 23.41% from 20.55% of the devices based on the pristine SnO_2. The N-SnO_2 devices show an outstanding stability retaining 97.8% of the initial efficiency after steady-state output at a maximum power point for 600 s under standard AM1.5G continuous illumination without encapsulation, while less than 50% efficiency remains for the devices based on pristine SnO_2. This simple scalable strategy has shown great promise toward highly efficient and stable PSCs.

KEYWORDS

electron transport layer, N doping, perovskite solar cell, SnO_2

1 | INTRODUCTION

Halide perovskite solar cells (PSCs) have attracted great attention in the last decade; the power conversion efficiency (PCE) has increased rapidly from 3.8% to 25.5%.[1–4] As a key component, electron transport layer (ETL) plays an important role in the performance of devices, which extracts electrons from the perovskite light-absorbing layer to transfer them to the cathode, prevents hole from transferring to the cathode, and reduces the interface charge accumulation and nonradiation recombination.[5–7] Meanwhile, the long-term stability of PSCs is strongly affected by ETLs.[8,9]

Various metal oxide semiconductors have been employed as ETLs, such as TiO_2,[10] ZnO,[11] WO_3,[12] and SnO_2.[13,14] Especially, the latter has been investigated extensively in PSCs due to its high transmittance, wide bandgap, and high electron mobility. SnO_2 thin films can be fabricated by electrochemical deposition,[15] atomic layer deposition (ALD),[16] sol–gel methods,[17–19] and so forth. Among them, chemical bath deposition (CBD) method is the most promising method to prepare the SnO_2 ETLs, as it is a simple and low-temperature process and easy to scale up. However, SnO_2 crystals made by CBD naturally contain defects with undesirable charge-trap states, resulting in nonnegligible hysteresis, low fill factor (FF), and poor stability for PSCs.[2,20]

Element doping can effectively regulate defects in SnO_2 nanocrystals, as well as the conductivity and band structure. The SnO_2 nanocrystals have been doped with metal elements, such as Sb,[21] Mo,[22] Al,[23] Ga,[24] Zr,[25] and La,[26] and nonmetal elements, such as F,[27] P,[28] and Cl.[29] Bu et al. demonstrated that element doping improved the conductivity of SnO_2 ETLs, decreased the energy barrier between SnO_2/perovskite interface, and enabled an increase in the PCE from 19.01% to 20.69%.[30] Recently, cobalt chloride hexahydrate ($CoCl_2{\cdot}6H_2O$) was introduced into SnO_2 ETLs to manage the detrimental defects and band structure. With the favorable energy level alignment and charge extraction, an enhanced open-circuit photovoltage (V_{oc}) up to 1.20 V was achieved along with an improved stability.[31] Although most of the research was focused on the ETLs prepared by spin-coating method that is unscalable, the doping technique has shown its superiority in improving the performance of SnO_2 ETLs.

Here, we report highly efficient and stable planar PSCs based on N-doped SnO_2 ETLs through the introduction of NH_4Cl in a CBD method, reaching a PCE over 23% with a high FF of 0.82 and a V_{oc} of 1.155 V, which benefit from favorable energy level alignment between ETL and perovskite, accelerated extraction and transport of electrons, and suppressed charge recombination. The N doping also improves the stability due to the reduced defects, retaining 97.8% of the initial efficiency after steady-state output at a maximum power point for 600 s. This strategy represents a breakthrough as it provided a simple and scalable way to deposit high-quality SnO_2 ETL for efficient and stable PSCs with efficiencies over 23%.

2 | RESULTS AND DISCUSSION

The SnO_2 film was fabricated by the CBD method; that is, soaking FTO glass substrates in an $SnCl_4$ aqueous solution bath at 90°C for 2 h.[32] The properties of the SnO_2 film are extremely important, directly affecting the final performance of prepared PSCs. Doping is a powerful technique to tune the properties of semiconductors. Here NH_4Cl was chosen as the N-doping source, and the SnO_2 films prepared by the addition of 250 mg NH_4Cl in bath solution are labeled as N-SnO_2. Figure 1A,B shows the scanning electron microscope (SEM) images of the SnO_2 films on FTO prepared by CBD. Both pristine SnO_2 and N-SnO_2 films are quite uniform and dense, indicating that the addition of NH_4Cl does not alter the morphology of SnO_2 films, so it is not surprising to see that the transmittance of the SnO_2 films is almost the same, as clearly shown in Figure S1.

To check whether N can be doped into SnO_2 by adding NH_4Cl, the x-ray photoemission spectroscopy (XPS) measurement was carried out. Figure 1C,D summarizes the XPS results on the pristine SnO_2 and the N-SnO_2. The corresponding Sn 3d 5/2 peaks appear at 487.06 and 486.89 eV, respectively (Figure 1C).[33] Sn 3d 5/2 peak shifts to lower binding energy with the N doping due to the lower electronegativity of N than O.[28] Meanwhile, the N-doped SnO_2 has a much stronger N signal than the pristine SnO_2 (Figure 1D), confirming the doping of N. A very weak peak observed in the undoped sample is due to the contamination from the ambient; that is, molecularly chemisorbed γ-nitrogen, which is confirmed by other researchers.[34,35] The N 1s high-resolution spectrum could be deconvoluted into two peaks, one peak at 399.6 eV attributed to anionic N incorporated in SnO_2 forming O-Sn-N linkages, and the other peak at 400.4 eV attributed to oxidized nitrogen. Quantitative estimates of the N/Sn ratios in N-SnO_2 film is ~2.0 at.%. The position of O 1s peak exhibits no significant change as shown in Figure S2, implying that the nature of oxygen is similar. As it is well known, proper band alignment is crucial for efficient ETLs in PSCs. Ultraviolet photoelectron spectroscopy measurement was performed to investigate the conduction band minimum (CBM) and valence band maximum (VBM) positions of the SnO_2 films and perovskite as displayed in Figure 2A,B. For the pristine SnO_2, N-SnO_2, and perovskite film, the cut-off binding energies ($E_{cut\text{-}off}$) are 16.62, 16.65, and 16.30 eV, respectively. Based on the equation of $E_{VBM} = 21.22 - (E_{cut\text{-}off} - E_{set\text{-}on})$,[36]

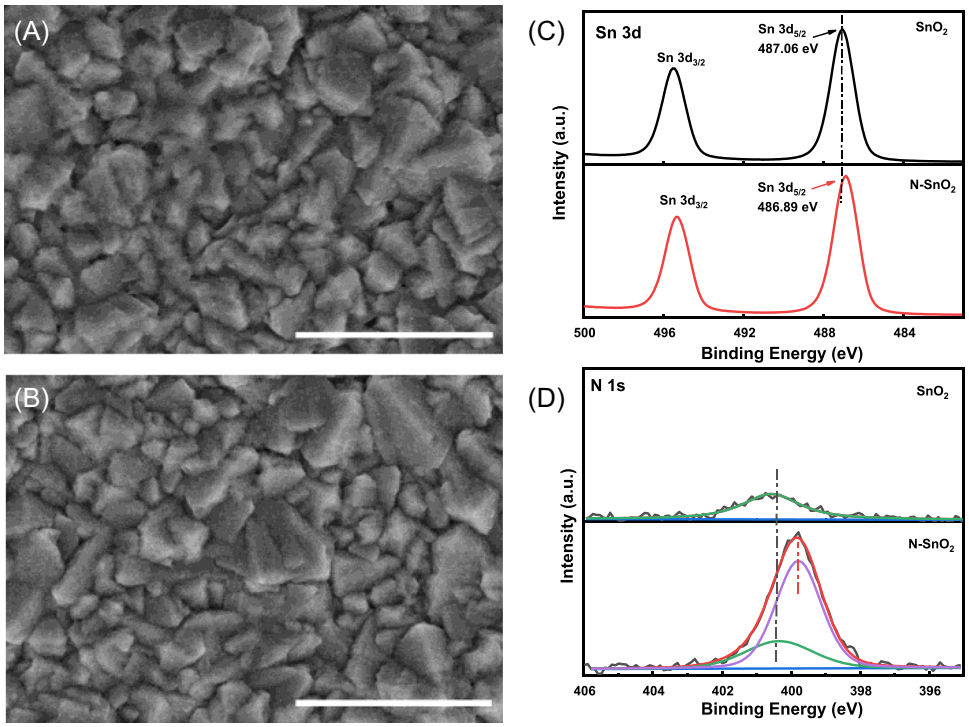

FIGURE 1 Scanning electron microscope images of (A) the pristine SnO_2 film and (B) the N-SnO_2 film. The scale bars are 1 μm. The XPS spectra of the pristine SnO_2 and N-SnO_2 films: (C) Sn 3d and (D) N 1s

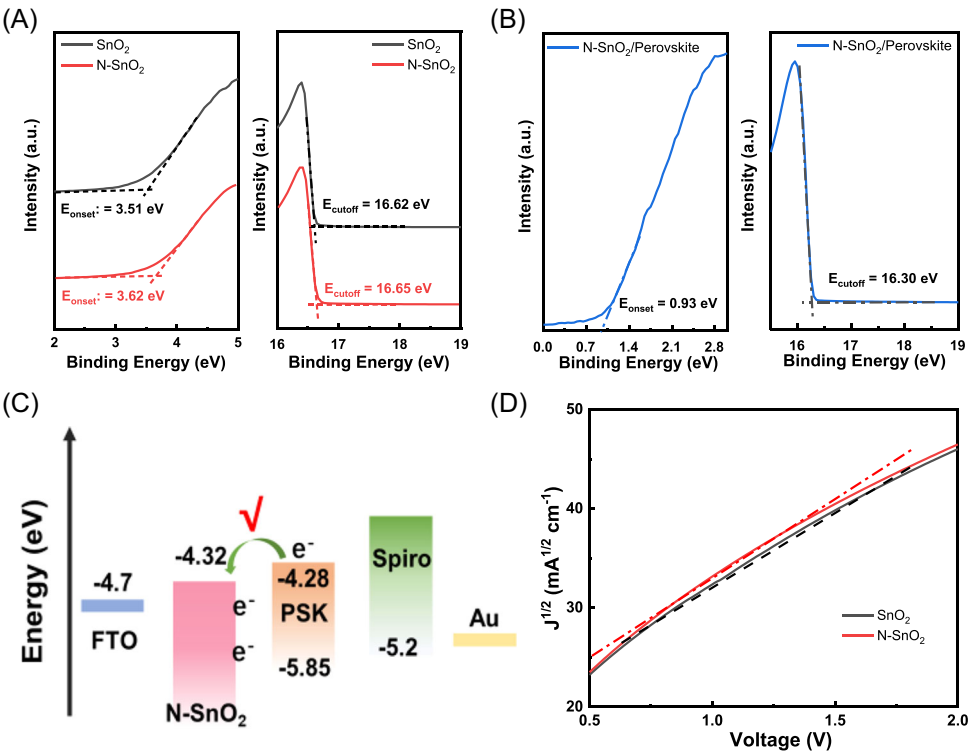

FIGURE 2 Ultraviolet photoelectron spectroscopy spectra of (A) the pristine SnO_2/N-SnO_2 and (B) the perovskite deposited on the N-SnO_2. (C) Band level diagram of devices based on the N-SnO_2 electron selective layers. (D) *J*–*V* curves of the electron-only devices using the space charge-limited current model

the E_{CBM} of the pristine SnO_2, N-SnO_2, and perovskite film are determined to be −4.21, −4.32, and −4.28 eV, respectively. It is found the CBM of the pristine SnO_2 is slightly higher than that of the perovskite, which will somehow impede the extraction of electrons in the perovskite to the ETL. With the doping of N, the CBM (−4.32 eV) shifts downward a little lower than that of the perovskite (−4.28 eV), as clearly shown in the energy level diagram (Figure 2C) that is drawn according to the E_g of the N-SnO_2 (3.87 eV) and perovskite (1.57 eV) extracted from Tauc plots (Figure S3). Apparently, the N-SnO_2 would show a better performance than the pristine SnO_2 ETL, with a reduced interface energy barrier and suppressed nonradiative recombination.

Another important property of ETLs is electron mobility. To check the effect of the N doping on the electron mobility of the SnO_2 films, the space charge-limited current measurement (Figure 2D) was conducted,[37] showing that electron mobility of the N-SnO_2 is $7.153 \times 10^{-3}\,cm^2\,V^{-1}\,s^{-1}$, a little higher than that ($6.990 \times 10^{-3}\,cm^2\,V^{-1}\,s^{-1}$) of the pristine SnO_2. ETLs with higher electron mobility could effectively transfer electrons, reduce the charge accumulation at the interface of ETL/perovskite, and then improve the FF of the device. Therefore, the N-SnO_2 is a good candidate for ETLs.

The quality of the ETL, including hydrophilicity, morphology, and attached chemical groups, directly determines the quality of the perovskite layer.[7] The UV-Vis spectra (Figure S4a) show a slightly stronger absorption of the perovskite deposited on the N-SnO_2 ETLs. Similarly, the XRD spectra in Figure S4b shows that doping slightly enhances the crystallinity of the perovskites. The SEM images of the perovskites (Figure 3A,B) and the corresponding statistics (Figure S5) show that the grain size of perovskites on the N-SnO_2 (1 μm) is larger than that on the pristine SnO_2 (0.8 μm). In general, a hydrophobic surface will result in enlarged grains of the deposited perovskites.[38] The contact angle images (Figure S6) clearly show a higher hydrophobicity of the N-SnO_2 surface.

To further examine the electron extraction ability of the ETLs, the steady-state photoluminescence (PL) spectra (Figure 3C) and normalized time-resolved PL (TRPL) spectra (Figure 3D) of the perovskite deposited on bare glass, SnO_2, and N-SnO_2 were measured. The strong steady PL of the perovskite on the bare glass indicates the high quality of the perovskite crystals. With the introduction of the SnO_2 ELTs, the PL is obviously suppressed. Compared with the pristine SnO_2, the N-SnO_2 has a stronger PL quench effect due to the better electron extraction and transportability. For the TRPL, the perovskite deposited on the bare glass has a slight decay process and a long lifetime, with an average lifetime of ~4.0 μs, while the average lifetime (Table S1) of the perovskites on ETLs was reduced by an order of magnitude, 0.313 μs (the pristine) and 0.271 μs (the doped), respectively. This further indicates that the N-SnO_2 is a much better electron extraction layer compared with the pristine SnO_2.

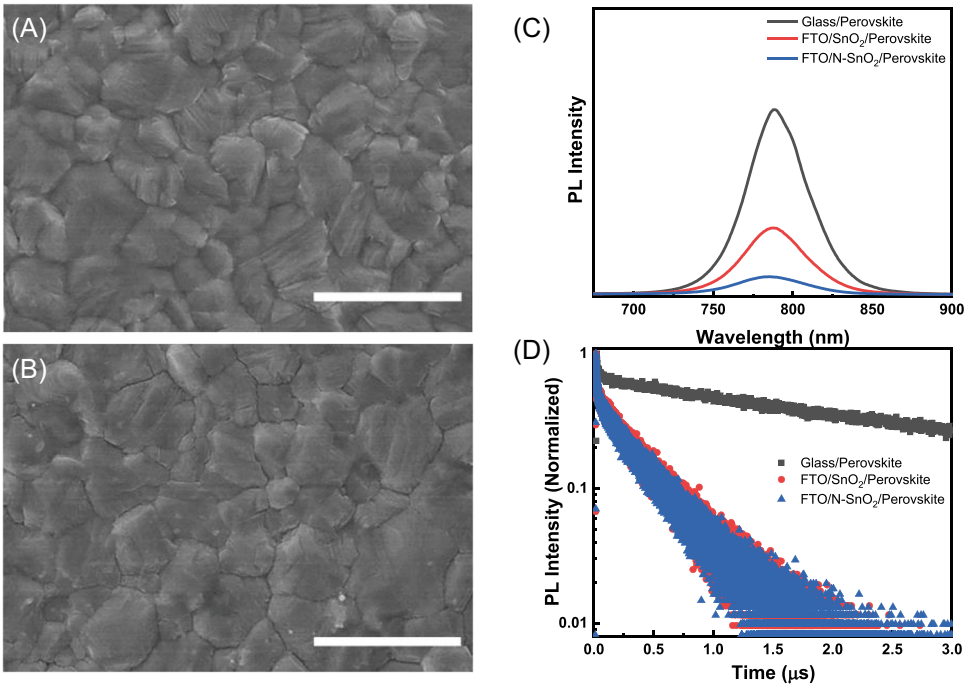

FIGURE 3 The scanning electron microscope images of perovskite films on (A) the pristine SnO_2 electron selective layer (ETL) and (B) the N-SnO_2 ETLs. The scale bars are 2 μm. (C) Steady-state photoluminescence (PL) and (D) time-resolved PL spectra of the perovskite films. The incident light is irradiated from the glass side

Then the SnO_2 ETLs were used to fabricate the complete devices, the cross-sectional SEM images of which are shown in Figure 4A,B. The related photovoltaic characteristics are listed in Table S2 and displayed in Figure S7. Figure 4C shows the champion *J–V* curves in forward and reverse scans under the illumination of AM1.5G 1 sun, and the corresponding photovoltaic characteristics are listed in Table 1. It is found that the pristine SnO_2 devices achieve a PCE of 20.55%, a V_{oc} of 1.081 V, a short-circuit photocurrent (J_{sc}) of 24.42 mA/cm^2, and a FF of 77.8% for the reverse scan. Interestingly, for the N-SnO_2 devices, the performance is significantly improved, achieving a high V_{oc} of 1.155 V, a J_{sc} of 24.81, a FF of 81.7%, and a PCE of 23.41% for the reverse scan. This is mainly due to the suitable interface contact and energy level alignment for the N-SnO_2 and perovskite as discussed, which reduces the interface defect density, accelerates the extraction of electrons, and reduces the energy loss caused by nonradiative recombination. The corresponding external quantum efficiency spectra are shown in Figure S8, and the integrated current density of devices based on the pristine SnO_2 and the N-SnO_2 is 23.93 and 24.10 mA/cm^2, respectively, consistent with J_{sc} from *J–V* curves.

To further understand the photovoltaic response and extract transfer resistance in the complete devices, electrical impedance spectroscopy was employed. The arc in the Nyquist plot (Figure 4D) of the devices measured at 0.8 V under dark conditions from 2 MHz to 0.5 Hz represents the charge recombination at the interface.[7] The N-SnO_2 devices have a recombination resistance (R_{rec}) of 3597 Ω, much larger than that (1122 Ω) of the pristine SnO_2 devices, revealing that the N-SnO_2 devices have a faster electron extraction and lower nonradiative recombination at the interface between the perovskite film and ETL.

The stability of the pristine SnO_2 and N-SnO_2 devices was also evaluated. The steady-state power output at a maximum power point was measured under standard AM1.5G 1 sun illumination for the unencapsulated devices, as shown in Figure 4E. The N-SnO_2 device retains

TABLE 1 Photovoltaic characteristics of the PSCs based on the pristine SnO_2 and the N-SnO_2 ETLs measured under simulated AM1.5G 1 sun illumination

Devices	Sweep	V_{oc} (V)	J_{sc} (mA/cm^2)	FF	PCE (%)
SnO_2	RS	1.081	24.42	0.778	20.55
	FS	0.918	24.43	0.478	10.73
N-SnO_2	RS	1.155	24.81	0.817	23.41
	FS	1.123	24.82	0.688	19.17

Abbreviations: ETLs, electron selective layers; FF, fill factor; PCE, power conversion efficiency; PSCs, perovskite solar cells.

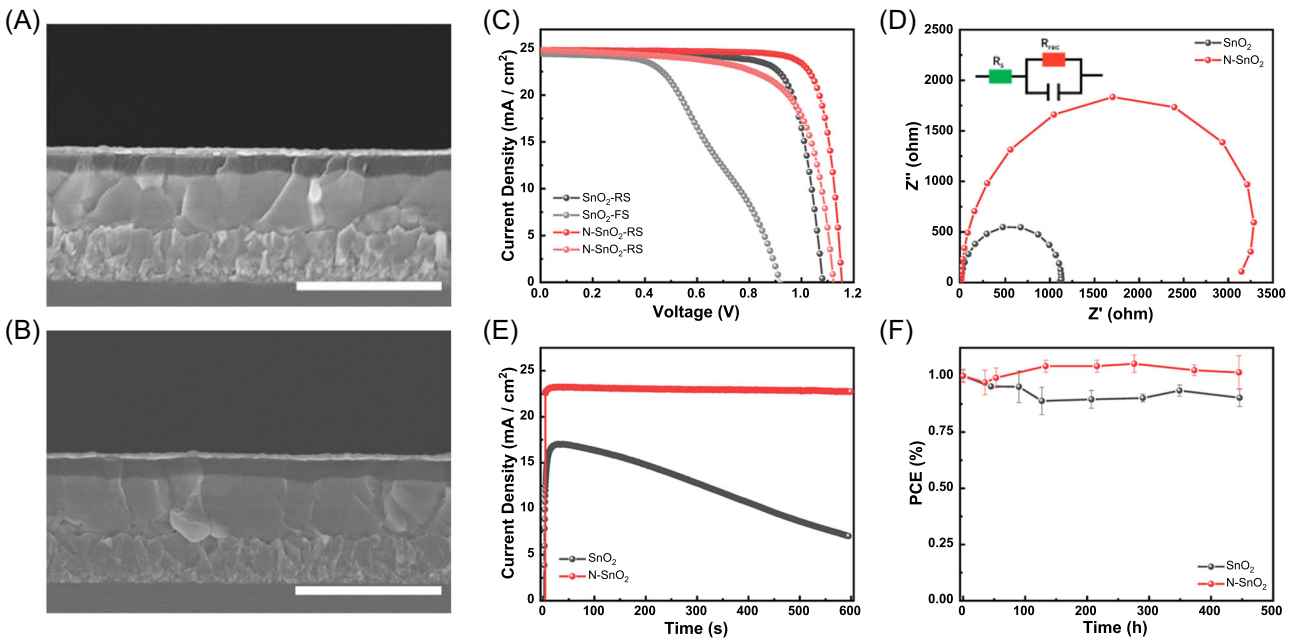

FIGURE 4 The cross-sectional scanning electron microscope images of the complete device based on (A) the pristine SnO_2 and (B) the N-SnO_2 electron selective layers (ETLs). The scale bars are 2 μm. (C) *J–V* curves of perovskite solar cells based on the pristine SnO_2 and N-SnO_2 ETLs. (D) Nyquist plots of devices measured at 0.8 V with a frequency range between 2 MHz and 0.5 Hz under dark. (E) Steady-state current density at the maximum power point for 600 s. (F) The long-term stability of the devices stored in dry air under dark

97.8% of the initial efficiency after 600 s, while the pristine SnO_2 device can only remain less than 50% of the initial efficiency. In addition, the devices were taken 20 cycles of *J*–*V* scan continuously under one sun illumination. The N-SnO_2 device shows a good stability, retaining ~98% of the initial efficiency, much better than the pristine SnO_2 with only 79% remaining (Figure S9). Impressively, the N-SnO_2 devices have good storage stability in the dark without any decrease in efficiency after 500 h storage, as shown in Figure 4F. These results demonstrate that the doping of N greatly improves the stability of SnO_2 deposited by CBD, and would be a useful strategy for scaling up PSCs.

3 | CONCLUSION

In summary, an effective strategy by employing NH_4Cl as N source doping into CBD SnO_2 has been developed for efficient and stable ETLs. The optimized SnO_2 film shows better electron mobility and electron extraction ability, and significantly increases the voltage and FF of the PSCs by effectively reducing interfacial charge accumulation and nonradiative recombination. Remarkably, the PCE of the champion device based on the N-SnO_2 ETL has been improved to 23.41% from 20.55%. The stability of the N-SnO_2 device without encapsulation is enhanced to retain 97.8% of the initial efficiency after steady-state output at a maximum power point for 600 s, much better than the pristine device that has only 50% efficiency left. This study provides a promising strategy toward efficient and stable PSCs with high-quality scalable ETLs.

ACKNOWLEDGMENTS

The Analytical and Testing Centre of Wuhan University of Technology and Hubei Key Laboratory of Low Dimensional Optoelectronic Material and Devices, Hubei University of Arts and Science are acknowledged for the XRD and SEM characterizations. This study is financially supported by the National Key Research and Development Plan (2019YFE0107200, 2017YFE0131900), National Natural Science Foundation of China (21875178, 52172230, 91963209), Fundamental Research Funds for the Central Universities (WUT: 202443004), and Foshan Xianhu Laboratory of the Advanced Energy Science and Technology Guangdong Laboratory (XDT2020-001, XHT2020-005).

CONFLICTS OF INTEREST

The authors declare no conflicts of interest.

ORCID

Fuzhi Huang http://orcid.org/0000-0002-8635-9262

REFERENCES

[1] Kojima A, Teshima K, Shirai Y, Miyasaka T. Organometal halide perovskites as visible-light sensitizers for photovoltaic cells. *J Am Chem Soc*. 2009;131:6050-6051.

[2] Yoo JJ, Seo G, Chua MR, et al. Efficient perovskite solar cells via improved carrier management. *Nature*. 2021;590:587-593.

[3] Jeong J, Kim M, Seo J, et al. Pseudo-halide anion engineering for alpha-$FAPbI_3$ perovskite solar cells. *Nature*. 2021;592:381-385.

[4] Kim G, Min H, Lee KS, Lee DY, Yoon SM, Seok SI. Impact of strain relaxation on performance of alpha-formamidinium lead iodide perovskite solar cells. *Science*. 2020;370:108-112.

[5] Rao H-S, Chen B-X, Li W-G, et al. Improving the extraction of photogenerated electrons with SnO_2 nanocolloids for efficient planar perovskite solar cells. *Adv Funct Mater*. 2015;25:7200-7207.

[6] Zhang X, Shi Z, Lu H, et al. Highly efficient planar perovskite solar cells via acid-assisted surface passivation. *J Mater Chem A*. 2019;7:22323-22331.

[7] Yang D, Yang R, Wang K, et al. High efficiency planar-type perovskite solar cells with negligible hysteresis using EDTA-complexed SnO_2. *Nat Commun*. 2018;9:3239.

[8] Leijtens T, Eperon GE, Pathak S, Abate A, Lee MM, Snaith HJ. Overcoming ultraviolet light instability of sensitized TiO_2 with meso-superstructured organometal tri-halide perovskite solar cells. *Nat Commun*. 2013;4:2885.

[9] Chen R, Cao J, Duan Y, et al. High-efficiency, hysteresis-less, UV-stable perovskite solar cells with cascade ZnO-ZnS electron transport layer. *J Am Chem Soc*. 2019;141:541-547.

[10] Etgar L, Gao P, Xue Z, et al. Mesoscopic $CH_3NH_3PbI_3/TiO_2$ heterojunction solar cells. *J Am Chem Soc*. 2012;134:17396-17399.

[11] Zhang DZ, Zhang XD, Bai S, et al. Surface chlorination of ZnO for perovskite solar cells with enhanced efficiency and stability. *Sol. RRL*. 2019;3:1900154.

[12] Mahmood K, Swain BS, Kirmani AR, Amassian A. Highly efficient perovskite solar cells based on a nanostructured WO_3-TiO_2 core-shell electron transporting material. *J Mater Chem A*. 2015;3:9051-9057.

[13] Shi S, Li J, Bu T, et al. Room-temperature synthesized SnO_2 electron transport layers for efficient perovskite solar cells. *RSC Adv*. 2019;9:9946-9950.

[14] Li J, Bu T, Liu Y, et al. Enhanced crystallinity of low-temperature solution-processed SnO_2 for highly reproducible planar perovskite solar cells. *ChemSusChem*. 2018;11:2898-2903.

[15] Ko Y, Kim YR, Jang H, Lee C, Kang MG, Jun Y. Electrodeposition of SnO_2 on FTO and its application in planar heterojunction perovskite solar cells as an electron transport layer. *Nanoscale Res Lett*. 2017;12:498.

[16] Lee Y, Lee S, Seo G, et al. Efficient planar perovskite solar cells using passivated tin oxide as an electron transport layer. *Adv Sci*. 2018;5:1800130.

[17] Anaraki EH, Kermanpur A, Steier L, et al. Highly efficient and stable planar perovskite solar cells by solution-processed tin oxide. *Energy Environ Sci*. 2016;9:3128-3134.

[18] Jung K-H, Seo J-Y, Lee S, Shin H, Park N-G. Solution-processed SnO_2 thin film for a hysteresis-free planar perovskite solar cell with a power conversion efficiency of 19.2%. *J Mater Chem A*. 2017;5:24790-24803.

[19] Jiang Q, Zhang L, Wang H, et al. Enhanced electron extraction using SnO_2 for high-efficiency planar-structure $HC(NH_2)_2PbI_3$-based perovskite solar cells. *Nat Energy*. 2017;2:16177.
[20] Jung EH, Chen B, Bertens K, et al. Bifunctional surface engineering on SnO_2 reduces energy loss in perovskite solar cells. *ACS Energy Lett*. 2020;5:2796-2801.
[21] Bai Y, Fang Y, Deng Y, et al. Low temperature solution-processed Sb:SnO_2 nanocrystals for efficient planar perovskite solar cells. *ChemSusChem*. 2016;9:2686-2691.
[22] Bahadur J, Ghahremani AH, Martin B, Druffel T, Sunkara MK, Pal K. Solution processed Mo doped SnO_2 as an effective ETL in the fabrication of low temperature planer perovskite solar cell under ambient conditions. *Org Electron*. 2019;67:159-167.
[23] Chen H, Liu D, Wang Y, et al. Enhanced performance of planar perovskite solar cells using low-temperature solution-processed Al-doped SnO_2 as electron transport layers. *Nanoscale Res Lett*. 2017;12:238.
[24] Ma Z, Zhou W, Xiao Z, et al. Negligible hysteresis planar perovskite solar cells using Ga-doped SnO_2 nanocrystal as electron transport layers. *Org Electron*. 2019;71:98-105.
[25] Noh YW, Lee JH, Jin IS, Park SH, Jung JW. Tailored electronic properties of Zr-doped SnO_2 nanoparticles for efficient planar perovskite solar cells with marginal hysteresis. *Nano Energy*. 2019;65:104014.
[26] Xu Z, Teo SH, Gao L, et al. La-doped SnO_2 as ETL for efficient planar-structure hybrid perovskite solar cells. *Org Electron*. 2019;73:62-68.
[27] Zhang S, Gu H, Chen S-C, Zheng Q. KF-doped SnO_2 as an electron transport layer for efficient inorganic $CsPbI_2Br$ perovskite solar cells with enhanced open-circuit voltages. *J Mater Chem C*. 2021;9:4240-4247.
[28] Wang D, Chen S-C, Zheng Q. Poly(vinylpyrrolidone)-doped SnO_2 as an electron transport layer for perovskite solar cells with improved performance. *J Mater Chem C*. 2019;7:12204-12210.
[29] Gong W, Guo H, Zhang H, et al. Chlorine-doped SnO_2 hydrophobic surfaces for large grain perovskite solar cells. *J Mater Chem C*. 2020;8:11638-11646.
[30] Tu B, Shao Y, Chen W, et al. Novel molecular doping mechanism for n-doping of SnO_2 via triphenylphosphine oxide and its effect on perovskite solar cells. *Adv Mater*. 2019;31:e1805944.
[31] Wang P, Chen B, Li R, et al. Cobalt chloride hexahydrate assisted in reducing energy loss in perovskite solar cells with record open-circuit voltage of 1.20 V. *ACS Energy Lett*. 2021;6:2121-2128.
[32] Bu T, Shi S, Li J, et al. Low-temperature presynthesized crystalline tin oxide for efficient flexible perovskite solar cells and modules. *ACS Appl. Mater. Interfaces*. 2018;10:14922-14929.
[33] Dutta D, Bahadur D. Influence of confinement regimes on magnetic property of pristine SnO_2 quantum dots. *J Mater Chem*. 2012;22:24545-24551.
[34] Chen C, Bai H, Chang C. Effect of plasma processing gas composition on the nitrogen-doping status and visible light photocatalysis of TiO_2. *J Phys Chem C*. 2007;111:15228-15235.
[35] Asahi R, Morikawa T, Ohwaki T, Aoki K, Taga Y. Visible-light photocatalysis in nitrogen-doped titanium oxides. *Science*. 2001;293:269-271.
[36] Chen J, Zhao X, Kim SG, Park NG. Multifunctional chemical linker imidazoleacetic acid hydrochloride for 21% efficient and stable planar perovskite solar cells. *Adv Mater*. 2019;31:e1902902.
[37] Yang D, Zhou X, Yang R, et al. Surface optimization to eliminate hysteresis for record efficiency planar perovskite solar cells. *Energy Environ Sci*. 2016;9:3071-3078.
[38] Bi C, Wang Q, Shao Y, Yuan Y, Xiao Z, Huang J. Non-wetting surface-driven high-aspect-ratio crystalline grain growth for efficient hybrid perovskite solar cells. *Nat Commun*. 2015;6:7747.

SUPPORTING INFORMATION

Additional supporting information can be found online in the Supporting Information section at the end of this article.

How to cite this article: Mo Y, Wang C, Zheng X, et al. Nitrogen-doped tin oxide electron transport layer for stable perovskite solar cells with efficiency over 23%. *Interdiscip Mater*. 2022;1:309-315. doi:10.1002/idm2.12022